COMMUNICATION

ChemComm
www.rsc.org/chemcomm

Dopant incorporation into garnet solid solutions—a breakdown of Goldschmidt's first rule†

W. van Westrenen,[ab] N. L. Allan,*[c] J. D. Blundy,[d] M. Yu. Lavrentiev,[c] B. R. Lucas[c] and J. A. Purton[e]

[a] *Geophysical Laboratory, Carnegie Institution of Washington, DC 20015, USA*
[b] *Institute for Mineralogy and Petrography, ETH Zürich, CH 8092, Switzerland*
[c] *School of Chemistry, University of Bristol, Cantock's Close, Bristol BS8 1TS, UK. E-mail: n.l.allan@bris.ac.uk*
[d] *Department of Earth Sciences, University of Bristol, Wills Memorial Building, Bristol BS8 1RJ, UK*
[e] *CLRC, Daresbury Laboratory, Warrington, Cheshire WA4 4AD, UK*

Received (in Cambridge, UK) 14th November 2002, Accepted 5th February 2003
First published as an Advance Article on the web 20th February 2003

Atomistic simulations suggest trace elements are more soluble in a 50 : 50 pyrope ($Mg_3Al_2Si_3O_{12}$)–grossular ($Ca_3Al_2Si_3O_{12}$) garnet mixture than in either end-member; consistent with partitioning experiments, and, contrary to Goldschmidt's first rule, large trace element cations may substitute for Mg^{2+}, small trace elements for Ca^{2+}.

A key problem in much of solid-state chemistry is the solubility of a trace element or dopant in a given material, and the non-ideality of the resulting solution. The pioneering work of Goldschmidt[1] established that principal controls on substitution are the mismatch in ionic radius and charge between substituent and host. Goldschmidt's first rule states that the most soluble dopants are those most similar in radius and charge to the host ion at a given site. A quantitative foundation has been provided by atomistic simulation techniques; for a wide range of end-member oxides[2] and silicates,[3] calculated solution energies vary parabolically with ionic radius (for given charge), with a minimum close to the radius of the host.

Surprisingly little attention has been paid to trace-element incorporation in solid solutions and natural samples. Existing models invoking 'forbidden zones'[4] around a given element often fail badly,[5] making an evaluation of the effects of solution formation on trace element energetics highly desirable. Here we report simulations of trace element incorporation in silicate garnets, and specifically at the dodecahedral X-sites of pyrope (Py, $Mg_3Al_2Si_3O_{12}$), grossular (Gr, $Ca_3Al_2Si_3O_{12}$) and Py–Gr solid solutions. These are of particular interest since experimental garnet-melt trace element partitioning data indicate that intermediate Py–Gr mixtures are anomalous in that behaviour is not intermediate between that of the pure end-members.[6] We calculate the energetics of substitution for a number of divalent trace elements. Non-Coulombic two and three-body potentials, and atomic charges, were taken from previous studies.[7,8,9] Agreement between observed and computed structural parameters for the garnet end-members is very satisfactory.†

Simulations of solutions with discrete Mg and Ca sites were carried out for $Py_{96}Gr_4$, $Py_{50}Gr_{50}$, and Py_4Gr_{96}. Possible cation orderings in the solid solution were examined in detail. Unusually, as in ref. 10, ordering is dominated by the third-nearest-neighbour interaction between cations at the centre of two dodecahedra that share edges with the *same* SiO_4 tetrahedron. This interaction (denoted d_3, highlighted in Fig. 1) is repulsive for *like* cations (Mg^{2+}–Mg^{2+} and Ca^{2+}–Ca^{2+}). The garnet polyhedral network constrains the structure such that rigid-unit modes involving rigid rotations of the polyhedra are not permitted.[10] When an X-site cation is replaced all polyhedra are therefore distorted, with the largest distortion in the two SiO_4 tetrahedra sharing edges with the dodecahedron containing the new cation.

For $Py_{50}Gr_{50}$, we examined fifteen different arrangements of Mg and Ca ions.[11] The first of these (configuration 1) avoided all energetically unfavourable Mg^{2+}–Mg^{2+} and Ca^{2+}–Ca^{2+} third-nearest-neighbour pairs. In the remaining configurations the X-site had a range of different first, second and third-nearest neighbours. Configuration 1 was lowest in energy. The others were higher in energy by 1–2 kJ mol^{-1}, suggesting configurations with unfavourable third-neighbour interactions are nevertheless energetically accessible at elevated temperatures.

Simulated structures were used as a basis for defect energy calculations.[12] The total energy of the defective system was minimised by allowing the surrounding ions to relax to accommodate the misfit dopant cation, using the two-region approach.[13] All simulations are in the static limit; defect energies, U_{def}, in this limit are in close agreement with defect enthalpies at elevated temperatures.[14]

For $Py_{50}Gr_{50}$ we examined substitutions for different local Mg–Ca distributions around the central X-site to study explicitly the effects of local ordering on dopant incorporation.† This included all possible nearest-neighbour and third-neighbour orderings and a large number of second-neighbour orderings. Solution energies U_{sol} for trace element J^{2+} at a Ca^{2+} site in $Py_{50}Gr_{50}$ relate to the equation:

$$JO(s) + Ca_{1.5}Mg_{1.5}Al_2Si_3O_{12}(s) = JCa_{0.5}Mg_{1.5}Al_2Si_3O_{12}(s) + CaO(s);\ U_{sol} = U_{def}(J_{Ca}) + U_{latt}(CaO) - U_{latt}(JO),$$

where U_{latt} denotes the lattice energy of the binary oxide.[15] Analogous equations apply for other compositions and for Mg^{2+} substitution.

Table 1 lists the lowest values of U_{sol} for Ni^{2+}, Fe^{2+}, Mn^{2+}, Sr^{2+} and Ca^{2+} in $Py_{50}Gy_{50}$. The new trace element optimises its *local* environment. Since there are no rigid unit modes, any tilting or rotation of a polyhedron in the framework to accommodate a trace element requires the same motion of all

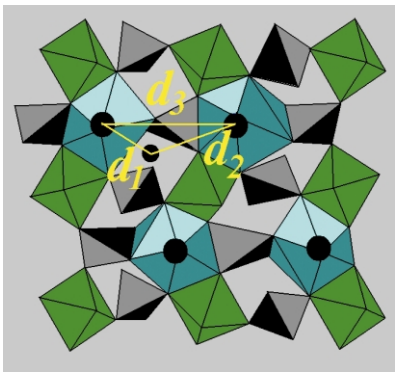

Fig. 1 The garnet structure. Alternating isolated SiO_4 tetrahedra (black) and AlO_6 octahedra (green) form a three-dimensional corner-sharing network. Resulting cavities form dodecahedra (blue) containing Mg or Ca cations. First (d_1), second (d_2) and third-nearest neighbour (d_3) cation–cation distances are highlighted.

† Electronic supplementary information (ESI) available: (1) comparison between observed and calculated structural parameters of the end-members pyrope and grossular. (2) GULP input file for configuration 1. See http://www.rsc.org/suppdata/cc/b2/b211249c/

DOI: 10.1039/b211249c

Table 1 Calculated lowest solution energies (kJ mol^{-1}) in pyrope (Py), grossular (Gr) and $Py_{50}Gr_{50}$. Column headed X specifies the cation replaced in $Py_{50}Gr_{50}$, and subsequent columns denote the first and third neighbours of the trace element in the solid solution.

Element	Solution energy (Py)	Solution energy (Gr)	Solution energy ($Py_{50}Gr_{50}$)	X	Nearest neighbours	Third nearest neighbours
Ni	2.6	28	−50	Ca	4 × Mg	2 × Ca
Fe	−11.9	0.3	−60	Ca	2 × Mg 2 × Ca	2 × Ca
Mn	0	−15	−51	Ca	2 × Mg 2 × Ca	2 × Ca
Sr	202	80	56	Mg	4 × Ca	2 × Mg
Ba	462	266	252	Mg	4 × Ca	2 × Mg

polyhedra, and the collective distortion involved is high in energy. Much lower in energy is the distortion of the tetrahedra and octahedra that are direct neighbours of the trace element.

Small changes in environment lead to relatively large changes in U_{def} and thus in U_{sol}, which show some remarkable features. The U_{sol} at certain Mg^{2+} and Ca^{2+} sites become comparable. The calculated solution energy for the largest ion, Ba^{2+}, at a Mg site in Py_4Gr_{96} is comparable to that at a Ca site in grossular itself. The lowest value of U_{sol} for the smallest ion, Ni^{2+}, is at a Ca^{2+} site in $Py_{96}Gr_4$ and is considerably lower that that for Ni^{2+} substitution in the end-members.

The local environment of the X-site is crucial. Consider the values for Ba^{2+}. The four first neighbours influence the solution energy U_{sol} in that it is slightly smaller if the host ion is surrounded by larger ions. The third-nearest neighbour shell also has a particularly large influence. If substitution of the X site cation removes an unfavourable third-neighbour interaction by introducing a size mismatch, both U_{def} and U_{sol} are lower, as the overall compression or extension of the tetrahedron between the two dodecahedra is reduced. U_{sol} for replacement of a Mg^{2+} by Ba^{2+} is ≈20–40 kJ mol^{-1} lower if first neighbours are all Ca as opposed to Mg. However, the solution energy varies by as much as 75 kJ mol^{-1} depending on the nature of the third neighbour. Overall the lowest solution energies of Ba^{2+} at an Mg and at a Ca site are 252 kJ mol^{-1} and 290 kJ mol^{-1} respectively.

These values are remarkable as they indicate the most favourable substitution site for the large Ba^{2+} in $Py_{50}Gr_{50}$ is not necessarily a Ca^{2+} site, as expected from ion size considerations. Substitution in $Py_{50}Gr_{50}$ can also take place at a Mg site depending on local environment. For comparison the solution energies of Ba^{2+} in pure pyrope and grossular are 462 kJ mol^{-1} and 266 kJ mol^{-1} respectively. The variation in calculated U_{sol} along the Py–Gr join (Fig. 2, top) is thus non-linear, with values for $Py_{50}Gr_{50}$ lower than those for either end-member. This results in a predicted higher solubility of Ba^{2+} (and Sr^{2+}) in $Py_{50}Gy_{50}$ than expected from interpolation between the end-members.

Defect energies for Ni^{2+}, Fe^{2+} and Mn^{2+} can be rationalised similarly. Introducing one of these dopants at an X-site where both third neighbours are Ca^{2+} is favoured relative to a site with two Mg^{2+} third neighbours, due to the removal of the effective repulsion between the dopant and its third-neighbour (Mg^{2+}) similar in size. Again, this is not in line with simple ion size considerations. This proposed link between dopant distribution and local Ca–Mg ordering is testable using EXAFS.

A plot of solution energy *vs.* ionic radius[16] (Fig. 2, bottom) summarises our conclusions. All divalent dopants are more soluble in $Py_{50}Gy_{50}$ than in the end-members. Large ions may substitute preferentially for a Mg^{2+} (with two Mg^{2+} third neighbours) rather than a Ca^{2+}, and small ions for a Ca^{2+} (with two Ca^{2+} third neighbours) rather than a Mg^{2+}. Goldschmidt's first rule thus breaks down for the garnet solid solution. It also provides an explanation for the anomalous trace-element partitioning behaviour of the solution,[6] since the lower solubilities cause a broadening of the solution energy *vs.* radius

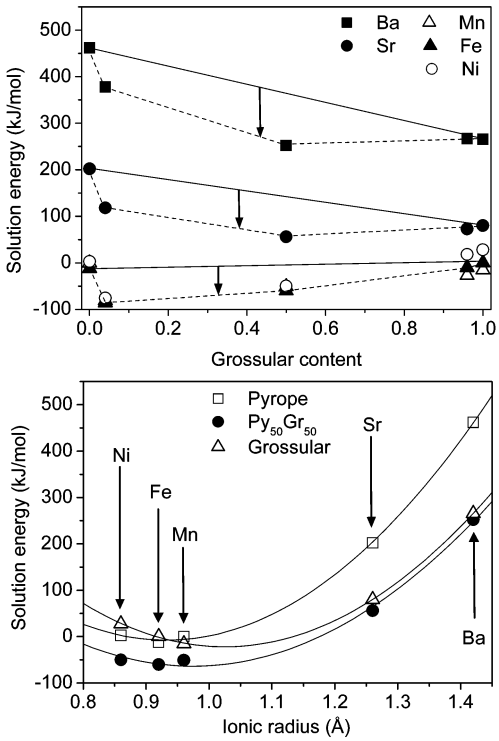

Fig. 2 *(top)* Variation of solution energies for five divalent trace elements across the pyrope–grossular join. Arrows indicate the solution energies in solid solutions are significantly lower than expected from a linear interpolation between end-member values (see dashed lines). *(bottom)* Solution energies *vs.* ionic radius[16] for pyrope (Py), grossular (Gr), and $Py_{50}Gr_{50}$.

curve, consistent with experiment. Although *structurally* the Ca and Mg sites remain clearly distinct in garnet solid solutions, *energetically* they may appear equivalent depending on the local environment.

This work was supported by SNF grant 2100-066903, EPSRC grant GR/M53899, and HEFCE JREI awards.

Notes and references

1 V. M. Goldschmidt, *J. Chem. Soc. (London)*, 1937, **140**, 655.
2 For example, N. L. Allan and W. C. Mackrodt, *Adv. Solid State Chem.*, 1993, **3**, 221.
3 For example, N. L. Allan, J. D. Blundy, J. A. Purton, M. Yu. Lavrentiev and B. J. Wood, in *Solid Solutions in Silicate and Oxide Systems*, ed. C. A. Geiger, EMU Notes in Mineralogy 3, Eötvös University Press, Budapest, 2001, pp. 251–302.
4 For example, J. T. Ilyama, *Bull. Soc. Fr. Mineral. Cristallogr.*, 1974, **97**, 143; R. C. Newton and B. J. Wood, *Am. Mineral.*, 1980, **65**, 733.
5 A. Bosenick, M. T. Dove and C. A. Geiger, *Phys. Chem. Min.*, 2000, **27**, 398.
6 W. van Westrenen, J. Blundy and B. Wood, *Am. Min.*, 1999, **84**, 838.
7 J. A. Purton, N. L. Allan, J. D. Blundy and E. A. Wasserman, *Geochim. Cosmochim. Acta*, 1996, **60**, 4977.
8 J. A. Purton, N. L. Allan and J. D. Blundy, *Geochim. Cosmochim. Acta*, 1997, **61**, 3927.
9 W. van Westrenen, N. L. Allan, J. D. Blundy, J. A. Purton and B. J. Wood, *Geochim. Cosmochim. Acta*, 2000, **64**, 1629.
10 A. Bosenick, M. T. Dove and C. A. Geiger, *Phys. Chem. Min.*, 2000, **27**, 398.
11 For a detailed Monte Carlo study see M. Lavrentiev, W. van Westrenen, N.L. Allan and J.A. Purton, in preparation.
12 All calculations were carried out using the GULP code; J. D. Gale, *J. Chem. Soc., Faraday Trans*, 1997, **93**, 629.
13 C. R. A. Catlow and W. C. Mackrodt, in *Computer simulation of solids*, ed. C. R. A Catlow and W. C. Mackrodt, Springer-Verlag-Heidelberg-Berlin, 1982, ch. 1, pp. 3–20.
14 M. B. Taylor, G. D. Barrera, N. L. Allan, T. H. K. Barron and W. C. Mackrodt, *Faraday Discuss*, 1997, **106**, 377.
15 Lattice energies for the binary oxides, obtained with the same inter-ionic potentials as used in the garnet simulations, are given in ref. 3.
16 Ionic radii from R. D. Shannon, *Acta Cryst A*, 1976, **32**, 751.